Journal of Power Sources 195 (2010) 3605–3611

Contents lists available at ScienceDirect

Journal of Power Sources

journal homepage: www.elsevier.com/locate/jpowsour

$CoFe_2O_4$ spinel protection coating thermally converted from the electroplated Co–Fe alloy for solid oxide fuel cell interconnect application

Z.H. Bi, J.H. Zhu*, J.L. Batey

Department of Mechanical Engineering, Tennessee Technological University, Box 5014, Cookeville, TN 38501, USA

ARTICLE INFO

Article history:
Received 25 September 2009
Received in revised form 2 December 2009
Accepted 3 December 2009
Available online 11 December 2009

Keywords:
$CoFe_2O_4$ spinel
Conductive coating
Metallic interconnect
Solid oxide fuel cell
Electroplating
Chromium migration

ABSTRACT

$CoFe_2O_4$ has been demonstrated as a potential spinel coating for protecting the Cr-containing ferritic interconnects. This spinel had an electrical conductivity of 0.85 S cm^{-1} at 800 °C in air and an average coefficient of thermal expansion (CTE) of 11.80×10^{-6} K^{-1} from room temperature to 800 °C. A series of Co–Fe alloys were co-deposited onto the Crofer 22 APU ferritic steel via electroplating with an acidic chloride solution. After thermal oxidation in air at 800 °C, a $CoFe_2O_4$ spinel layer was attained from the plated $Co_{0.40}Fe_{0.60}$ film. Furthermore, a channeled Crofer 22 APU interconnect electrodeposited with a 40-μm $Co_{0.40}Fe_{0.60}$ alloy film as a protective coating was evaluated in a single-cell configuration. The presence of the dense, Cr-free $CoFe_2O_4$ spinel layer was effective in blocking the Cr migration/transport and thus contributed to the improvement in cell performance stability.

Published by Elsevier B.V.

1. Introduction

Solid oxide fuel cells (SOFCs) have recently attracted tremendous interest because of their high efficiency, low pollution emission, and relatively flexible fuel choice. Recent progress in the development of planar intermediate-temperature SOFCs has made it possible to use metallic alloys as the interconnect material [1–9]. Several chromia-forming ferritic stainless steels, such as Crofer 22 APU, UNS 430 and ZMG 232 are particularly promising, as they offer the advantages of low raw material cost, excellent formability, high electrical and thermal conductivity, decent oxidation resistance, and thermal expansion match with adjacent cell components. However, there are two major challenges associated these ferritic alloys, including electrical resistance increase over time due to continuous oxidation at elevated temperatures and evaporation/migration of the Cr species from the interconnect alloy into the cathode, both of which lead to severe degradation in cell performance.

Protective and conductive oxide coatings have been proposed to reduce the Cr volatilization of the Cr-containing interconnect alloys by acting as a barrier for Cr migration/transport. Perovskite coating materials, such as $(LaSr)CoO_3$, $(LaSr)CrO_3$, $(LaSr)MnO_3$, have been studied extensively and overall they are not very effective because of diffusion of chromium through the coatings and potential formation of thick interfacial reaction layers [7,10–12]. Several conductive spinel coatings, such as $MnCo_2O_4$, $Mn_{1.5}Co_{1.5}O_4$, $(Cu,Mn)_3O_4$, etc. were found to be more promising to block Cr migration [13–16]. A number of coating techniques have been utilized to synthesize the spinel coatings, including sputtering, plasma spray, air spray, reactive slurry coating, electroplating followed by thermal oxidation, etc.

Among the various proposed coating techniques, electroplating of a metal or alloy precursor layer on the interconnect alloy followed by *in situ* oxidation at typical SOFC operating temperature to thermally convert the precursor layer into a spinel coating is a simple and cost-effective approach, which can be utilized to coat almost any surface geometry with simple surface preparation. For example, a cobalt layer electroplated on the UNS 430 stainless steel was thermally oxidized to form Co_3O_4 which reacted with Fe and Cr to achieve a surface layer of mixed spinels [17,18]. While this layer could significantly retard Cr evaporation, the Cr volatility problem was not completely eliminated, as Cr was still present in the spinels. Conductive spinels coatings of $(Cu,Mn)_3O_4$, $(Co,Mn)_3O_4$, and $(Cu,Fe)_3O_4$ were also synthesized on the surface of Fe–Cr stainless steels by electroplating the Cu, Mn and Fe layers in different bath solutions, followed by thermal conversion of the plated layers into corresponding spinels [19–21]. Due to significant difference between the standard electrode potentials of Co^{2+}/Co ($-0.28\,V_{SCE}$) and Mn^{2+}/Mn ($-1.18\,V_{SCE}$), it is difficult to electrodeposit the Mn–Co alloys, even though limited success has been reported with DC or pulse plating method [22–24]. Compared with Mn^{2+}/Mn, the standard electrode potential of Fe^{2+}/Fe

* Corresponding author. Tel.: +1 931 372 3186; fax: +1 931 372 6340.
E-mail address: jzhu@tntech.edu (J.H. Zhu).

0378-7753/$ – see front matter. Published by Elsevier B.V.
doi:10.1016/j.jpowsour.2009.12.011

Table 1
Bath concentration and sacrificial anode composition for electrodeposition of the Co_xFe_{1-x} alloy film. The bath temperature was 65–70 °C, the bath pH was 1.70–2, and the plating current density was 20 mA cm^{-2}.

	Bath-1	Bath-2	Bath-3	Bath-4	Bath-5
$CoCl_2$ (M)	0.3	0.5	0.6	0.8	1.0
$FeCl_2$ (M)	1.2	1.0	0.4	0.2	–
$CaCl_2$ (M)	1.0	1.0	1.0	1.0	1.5
L-Ascorbic acid (M)	0.05	0.05	0.05	0.05	0.05
Anode composition	$Co_{0.33}Fe_{0.67}$	$Co_{0.40}Fe_{0.60}$	$Co_{0.60}Fe_{0.40}$	$Co_{0.80}Fe_{0.20}$	Pure Co

($-0.44\,V_{SCE}$) is relatively close to that of Co^{2+}/Co; therefore, co-deposition of the Co–Fe alloy via electroplating is more feasible and controllable. Indeed, the Co–Fe alloy thin films (<5 μm) prepared by electrodeposition was extensively studied in the past due to their wide range of applications in magnetic devices. According to the previous works [25,26], the Co–Fe alloy composition can be readily controlled via adjustment of the electroplating solution concentration.

In this work, the potential of the $CoFe_2O_4$ spinel coating for protecting the ferritic interconnect was assessed via measurement of its electrical conductivity and coefficient of thermal expansion (CTE). Electroplating of a series of Co_xFe_{1-x} alloy layer on Crofer 22 APU steel and thermal conversion of the $Co_{0.4}Fe_{0.6}$ alloy layer into a $CoFe_2O_4$ spinel coating were also demonstrated. The effect of the electroplated $Co_{0.4}Fe_{0.6}$ layer on the performance of the Crofer 22 APU interconnect was evaluated by cell testing using an anode-supported cell with the $La_{0.8}Sr_{0.2}MnO_{3-\sigma}$ (LSM) cathode.

2. Experimental

The $CoFe_2O_4$ spinel powder was prepared by solid-state reaction. The appropriate amounts of Fe_2O_3 (Sigma–Aldrich, 99.999%) and Co_3O_4 (Sigma–Aldrich, 99.995%) powders were thoroughly mixed, pressed into pellets, and then calcined at 1000 °C. The reacted pellets were crushed and re-ground, followed by ball-milling for 0.5 h. The ball-milled powder with 0.5 wt.% PVB was pressed into rectangular bars (34 mm × 7 mm × 6 mm) at an applied stress of 75 MPa, followed by sintering at 1300 °C for 10 h to achieve ≥ 92.0% relative density. X-ray diffraction (XRD) was carried out using Cu Kα radiation to verify the phase structure. The electrical conductivity was measured by the standard four-probe DC method in air from 500 to 1000 °C. The average CTE was measured in air from room temperature to 800 °C with an Anter dilatometer (1700 Universal, Anter Corporation).

A number of rectangular samples (about 12 mm × 12 mm × 3 mm) were cut from the Crofer 22 APU sheet and polished with silicon carbide papers up to 600 grit. The coupons were ultrasonically cleaned with distilled water and acetone. Before electroplating, the coupons were pickled in 10% hydrochloric acid for 10 min. Acidic chloride solutions with different compositions were employed for plating to attain the Co_xFe_{1-x} alloy layers with different ratios of Co and Fe, as named Bath-1 to -5. The bath solution details and plating conditions are shown in Table 1. Note that different cast alloys with composition identical to the targeted plated layer were employed as the sacrificial anode to maintain the plating solution concentration.

The surface and composition of the Co_xFe_{1-x} alloy films in the as-plated and oxidized (at 800 °C in air for 100 h) conditions were examined using a scanning electron microscope (SEM, FEI XL30) attached with an energy-dispersive spectroscope (EDS). The phase structure of the $Co_{0.40}Fe_{0.60}$ alloy plated interconnect were also determined by XRD before and after cell testing.

For cell testing, a Crofer 22 APU sheet (3.0 mm thick) was machined into a current collector (interconnect) with channels to allow for air flowing to the cathode, as illustrated in Fig. 1. The interconnect substrate was electroplated using the same parameters for the $Co_{0.40}Fe_{0.60}$ alloy coating on the rectangular coupon. The current efficiency in electroplating (the percentage of the total current usefully employed for the cathodic deposition of the alloy film) was around 93% under such plating conditions.

The anode-supported single cell consisted of a 1.0-mm porous NiO-YSZ (yttria-stabilized zirconia) anode substrate as support, a 10-μm NiO-YSZ anode function layer, a 8-μm thin YSZ electrolyte layer, a 15-μm LSM-YSZ cathode interlayer, and a 50-μm LSM current collector. Note that NiO in the anode support and functional layer would be reduced to Ni during cell testing. The diameter of the anode and electrolyte assemble was 25 mm, the diameter and active area of the LSM cathode were 18 mm and 2.5 cm^2, respectively.

The button cell assembly was sealed onto an Al_2O_3 tube using the Al_2O_3 paste (Aremco Products, Inc.). Ni mesh and paste were used as anode current collector. The bare and $Co_{0.40}Fe_{0.60}$-plated Crofer 22 APU interconnects spot-welded with Pt wires were compressed onto the cathode using 10 psi pressure. For the baseline testing, Ag mesh and paste were used as cathode current collector, while Pt paste was used as a contact material for cell testing with channeled interconnects. The assembled cells were placed inside a furnace and heated to 800 °C in 2.5 h with H_2 + 3% H_2O on the anode side and air on the cathode side. The flow rates of H_2 and air were 50 and 500 ml min^{-1}, respectively. The cells were operated at a constant voltage of 0.7 V using an electronic load, with the current recorded as a function of time using a digital multimeter. After testing, the surface morphologies and cross-sectional views of the interconnects and cells were also analyzed by SEM/EDS.

3. Results and discussion

3.1. Electrical conductivity and CTE of $CoFe_2O_4$

The temperature dependence of the electrical conductivity for the $CoFe_2O_4$ spinel in air is shown in Fig. 2. A nearly linear relationship between $\ln(\sigma T)$ and $1/T$ was observed above 650 °C.

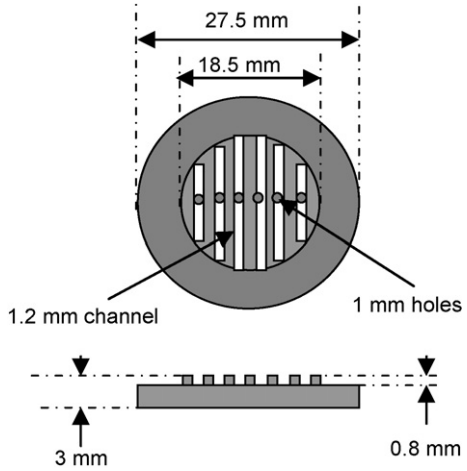

Fig. 1. Schematic of the channeled Crofer 22 APU interconnect.

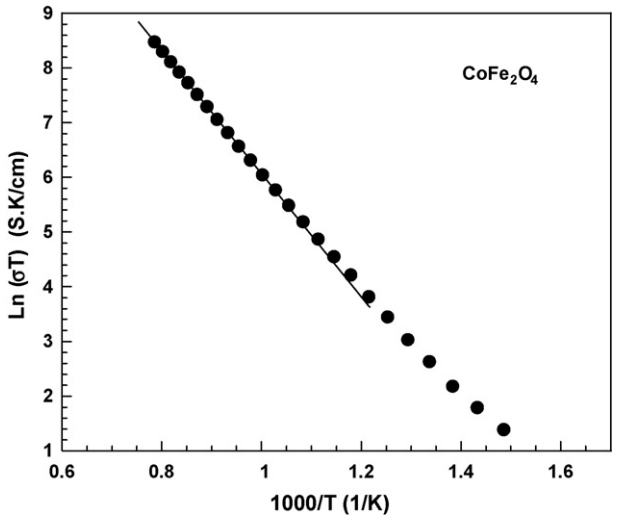

Fig. 2. Arrhenius plot of the electrical conductivity of $CoFe_2O_4$ from 400 to 1000 °C.

The electrical conductivity of the $CoFe_2O_4$ spinel was 0.11 and 0.85 S cm^{-1} at 600 and 800 °C, respectively, which is in good agreement with the value reported by Ling and Petric (e.g. 0.83 S cm^{-1} at 800 °C) [27]. This value is lower than that of the $(CuMn)_3O_4$ and $(Co,Mn)_3O_4$ spinels at 800 °C [28,29]. However, it is acceptable for the metallic interconnect protection layer, which is usually relatively thin, within 1–50 μm in thickness.

Also, the average CTE of the $CoFe_2O_4$ spinel was determined to be 11.8×10^{-6} K^{-1} from room temperature to 800 °C, which was close to that of the ferritic stainless steels such as Crofer 22 APU, ZMG 232, and E-Brite [30]. Apparently, both electrical conductivity and CTE of the $CoFe_2O_4$ spinel are adequate for it to be used as an alternative spinel protection coating for SOFC metallic interconnects.

3.2. Examination of the electrodeposited layer before and after oxidation

The surface morphologies of the electrodeposited layers from the Bath-2 and Bath-5 are shown in Fig. 3. All the Co_xFe_{1-x} films exhibited polyhedral crystallites with an average grain size of 10 μm except that the pure Co plated layer exhibited a mixture of acicular and polyhedral crystallites. The effects of deposition temperature, solution pH and L-ascorbic acid on the Co–Fe film morphology and crystal structure were studied by Park et al. [25]. According to their results, the size of polyhedral crystallites increased as the deposition temperature increased from 23 to 70 °C, with the polyhedral crystallite size of about 5 μm achieved for solution pH of 0.3–1.5 at 70 °C. Obviously, a larger crystallite size was obtained for our plated CoFe layer, which might be related to the thicker deposit layer for our samples.

The composition of the plated layer attained from different bath solutions, as determined by EDS, was plotted as a function of the Co:Fe ratio (atom) in the bath solution in Fig. 4. Clearly, it is relatively easy to achieve a desired alloy concentration by choosing the appropriate Co:Fe ratio in the bath solution. This linear behavior in the co-deposition of Co^{2+} and Fe^{2+} was also observed in the previous studies [26,31]. A cross-sectional view and EDS line scan of the Crofer 22 APU coupon with the electrodeposited $Co_{0.4}Fe_{0.6}$ alloy film are shown in Fig. 5(a) and (b), respectively. No crack or peel-off was observed in the plated layer. The plated layer was also very dense and uniform in thickness (around 40 μm) according to the surface morphology and cross-section view. The Co content of the plated Co–Fe alloy film was very uniform across the sample

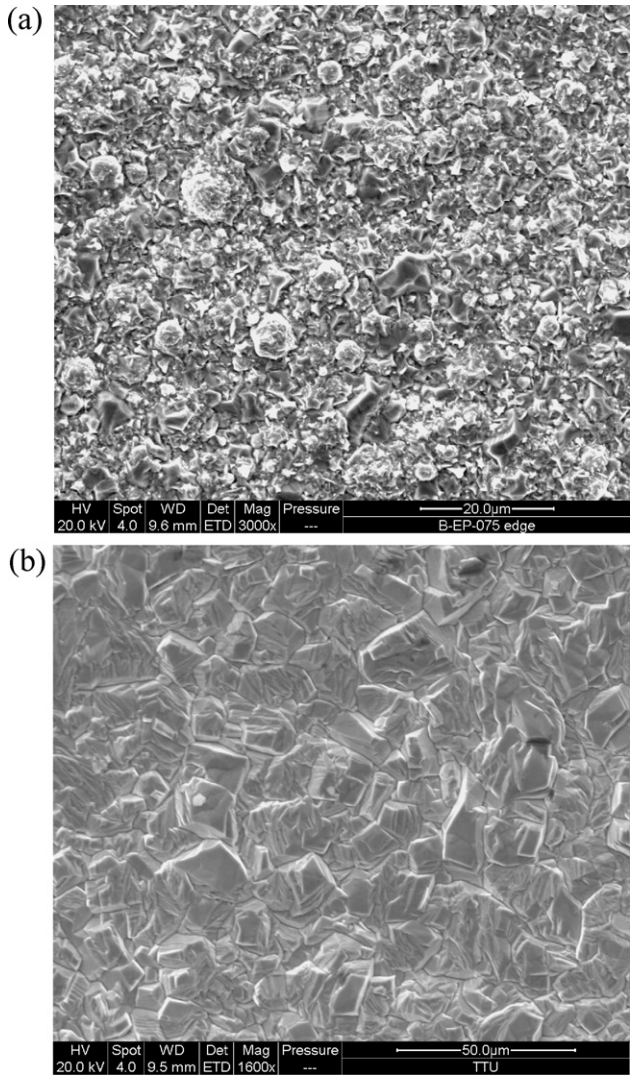

Fig. 3. Surface morphologies of the electrodeposited film of (a) pure Co and (b) $Co_{0.40}Fe_{0.60}$.

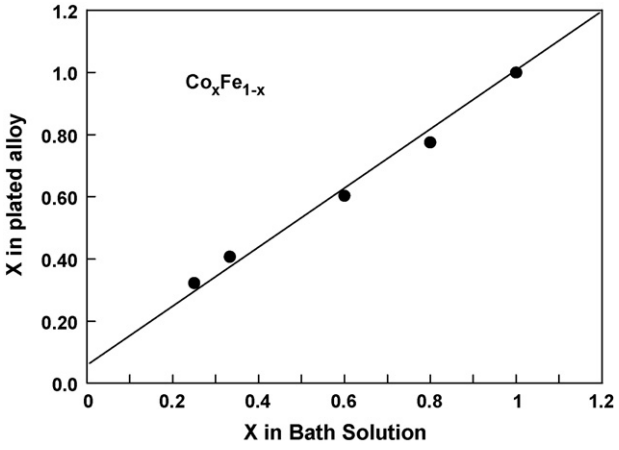

Fig. 4. The Co content in the electrodeposited Co_xFe_{1-x} layer as a function of the Co:Fe ratio in the bath solution.

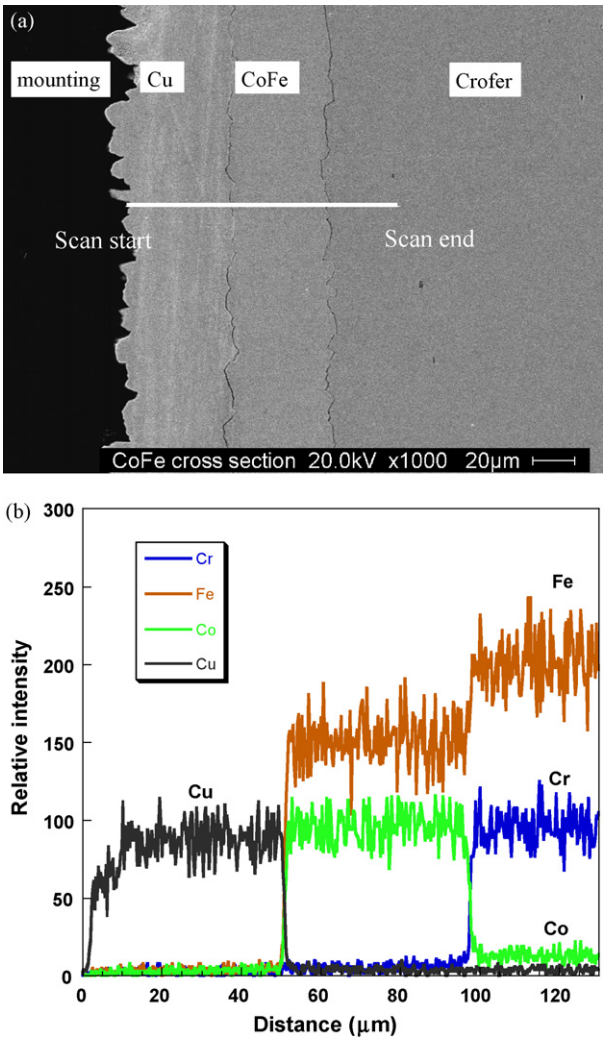

Fig. 5. Cross-sectional view (a) and EDS line scan (b) of the electrodeposited $Co_{0.40}Fe_{0.60}$ alloy film. Note that the Cu layer was added for improving the edge retention of the sample.

because the bath solution was relatively stable with the use of the sacrificial $Co_{0.40}Fe_{0.60}$ alloy as anode. Furthermore, the utilization of the Co–Fe alloy as the anode could avoid the formation of Fe(III) in the solution, as would be the case with platinum anode. The XRD spectrum of the electrodeposited $Co_{0.40}Fe_{0.60}$ alloy, as shown in Fig. 6(a), indicates that the deposited $Co_{0.40}Fe_{0.60}$ layer had the body-centered cubic (BCC) structure with the (1 1 0) preferred orientation, consistent with the earlier studies [25,26,31].

The surface composition of the oxidized Co_xFe_{1-x} layer, as determined by EDS, is shown in Table 2. According to the Co:Fe ratio in the surface oxide shown in Table 2, only the composition of the surface oxide formed from the $Co_{0.4}Fe_{0.6}$ layer was close to $CoFe_2O_4$. The XRD pattern taken on the oxidized surface of the $Co_{0.40}Fe_{0.60}$-plated coupon, as shown in Fig. 6(b), further confirms that the oxide scale thermally grown after exposure to air at 800 °C for 20 h was mainly the $CoFe_2O_4$ spinel phase with a small mount of Fe_3O_4. Therefore, the $Co_{0.40}Fe_{0.60}$ layer was selected to act as a protective coating for the Crofer 22 APU interconnect for additional in-cell testing.

Table 2
EDS analysis results of the oxidized surfaces of the bare and plated Crofer 22 APU coupons after oxidation in air at 800 °C for 100 h (in at.%).

	O	Cr	Mn	Fe	Co
Pure Co	51.6	–	–	1.4	47.0
$Co_{0.80}Fe_{0.20}$	50.0	–	–	4.0	46.0
$Co_{0.60}Fe_{0.40}$	48.2	–	–	30.9	20.9
$Co_{0.40}Fe_{0.60}$	46.4	–	–	35.9	17.6
$Co_{0.33}Fe_{0.67}$	50.6	–	–	33.3	16.1
Bare substrate	38.4	36.4	13.5	11.7	–

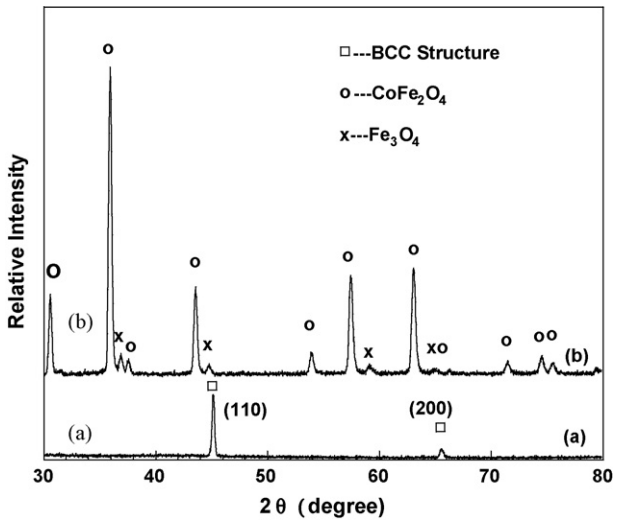

Fig. 6. XRD spectra of the $Co_{0.40}Fe_{0.60}$ alloy film deposited on Crofer 22 APU: (a) as-deposited, and (b) after oxidization for 10 h in air at 800 °C.

3.3. Cell performance with bare and $Co_{0.40}Fe_{0.60}$-plated interconnects

The results of the button cell tests are given in Fig. 7, where the power density versus time was plotted for the cells with Ag mesh, bare and $Co_{0.40}Fe_{0.60}$-plated Crofer 22 APU attached to the cathode, respectively. The baseline was conducted using the cell with the Ni and Ag meshes as anode and cathode current collector, respectively; the cell testing was terminated after 180-h cell operation, as the power density was very stable with a negligible degradation from 30 to 180 h.

From the baseline shown in Fig. 7, the typical initial "burn-in" of the LSM cathode was observed; after about 20-h cell operation, an essentially constant power density of around 490 mW cm^{-2} was maintained. Such "burn-in" behavior has been reported for

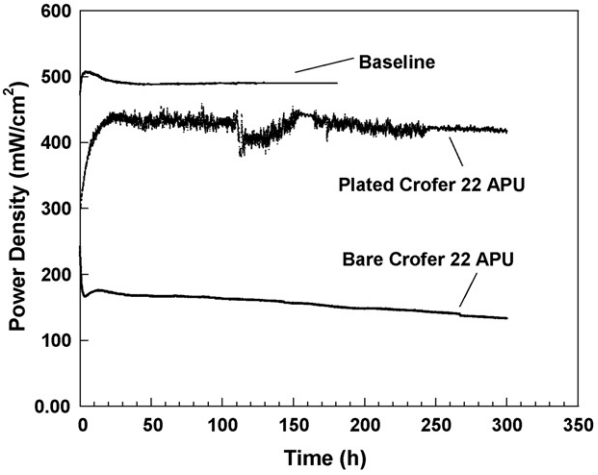

Fig. 7. Performance stability of the single cells with the bare and $Co_{0.40}Fe_{0.60}$-plated Crofer 22 APU interconnects. The baseline data from a single cell with Ag mesh/paste cathode current collector was also included for comparison.

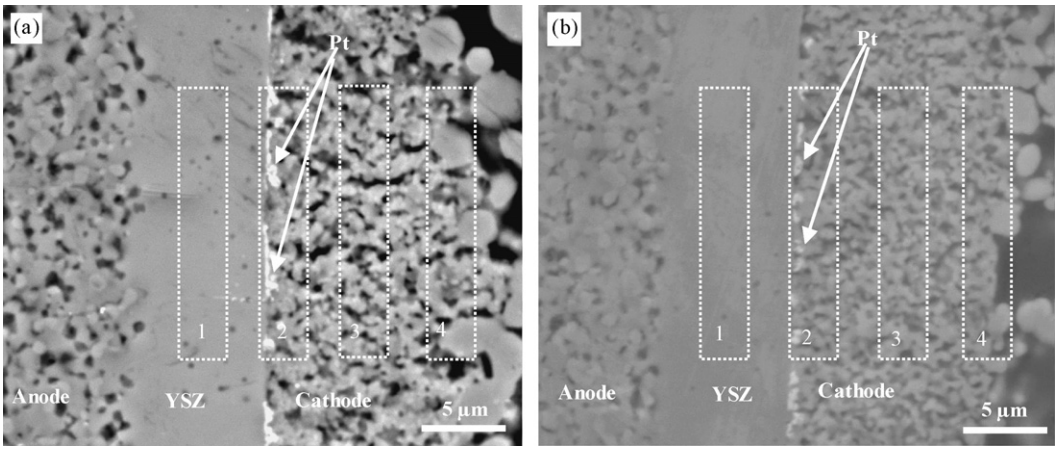

Fig. 8. SEM images of the cross-section of the Ni-YSZ/YSZ/LSM-YSZ/LSM cells after 300-h stability testing in air at 800 °C using (a) bare Crofer 22 APU; and (b) $Co_{0.40}Fe_{0.60}$-plated Crofer 22 APU as interconnects, respectively.

the cell with the Pt mesh and paste as current collector as well, which was related to the LSM cathode material as well as the sintering/migration of Pt particles [22,32]. The cells with bare and $Co_{0.40}Fe_{0.60}$-plated interconnects were operated for about 300 h. These cells exhibited similar power densities at the beginning of the tests, 295 and 243 mW cm^{-2}, respectively, which were around 40% lower than that of the cell with Ag mesh/paste as cathode current collector due to the fact that the contacting area between the interconnect and LSM cathode is half of that with Ag mesh/paste. The cell with the bare Crofer 22 APU interconnect exhibited significant decrease in power density in the first 4 h. Afterwards, the performance degradation slowed down with a relatively constant degradation rate; the power density decreased from 176 to 140 mW cm^{-2} during the remaining operation. The quick drop in cell performance at the beginning stage of our test is probably due to that the evaporated CrO_3 or $Cr_2(OH)_2O_6$ was reduced at the electrochemical active sites, thus blocking the oxygen reaction sites and leading to the rapid increase in both charge-transfer resistance and surface diffusion resistance of the LSM cathode [24,33]. The decrease in cell performance then slowed down and achieved a constant degradation rate of $\sim 3 \times 10^{-4}$ W cm^{-2} h^{-1} for the last 100 h, likely due to additional Cr transport as well as the ohmic resistance increase with continuous oxidation of the interconnect.

The performance of the cell with the $Co_{0.40}Fe_{0.60}$-plated interconnect exhibited a more drastic initial "burn-in", followed by stable performance at around 430 W cm^{-2}, slightly lower than the baseline. The stability in cell performance is likely due to the effectiveness of the $CoFe_2O_4$ spinel coating in blocking the Cr transport to the cathode. An unexpected furnace power outage disrupted the test temporarily at 100 h; however, the power density of the cell still was around 420 mW cm^{-2} after 310-h operation. The degradation rate of the cell with the $Co_{0.40}Fe_{0.60}$-plated Crofer 22 APU interconnect was about 3×10^{-5} W cm^{-2} h^{-1} for the last 100 h, which is approximately an order of magnitude lower than that of the cell with the bare interconnect. More importantly, the $Co_{0.40}Fe_{0.60}$ coating provided an initial increase in power density rather than the sharp decrease displayed by the cell with bare interconnect. This is most likely due to the blockage of Cr diffusion from the interconnect alloy to the cathode with the presence of the dense $Co_{0.40}Fe_{0.60}$ alloy layer and its subsequent conversion to a Cr-blocking $CoFe_2O_4$ spinel layer.

In order to provide further understanding regarding the different cell performances with the coated and uncoated interconnects, the cross-sections of the tested cells were analyzed by SEM/EDS. Fig. 8(a) and (b) shows the SEM images of the cross-sections of the single cells using bare and $Co_{0.40}Fe_{0.60}$-plated Crofer 22 APU interconnects after around 300-h stability testing at 800 °C. From Fig. 8(a) and (b), the Pt deposits (as confirmed by EDS) were clearly observed on the interface between the YSZ electrolyte and the cathode for the cells with both the bare and coated interconnects. The migration or deposition of Pt to the cathode–electrolyte interface can potentially catalyze the oxygen reduction reaction, which could lead to the cell performance increase during the initial cell testing. Similar result was reported in an earlier study by Simner et al. [32].

Significant differences in Cr distribution throughout the cell structures were observed for the cells with different interconnects. Table 3 lists the Cr content in the different regions of the test cells as indicated in Fig. 8. After 300-h operation at 800 °C, a maximum Cr content was found at the interface between the YSZ electrolyte and the LSM-YSZ cathode for the single cell with the bare Crofer 22 APU interconnect. However, near the interface between the cathode and LSM current collector region (i.e. Region 4), a relatively low Cr content was detected compared to that at the electrolyte/cathode interface, implying that the Cr poisoning was from Cr evaporation rather than a solid-state diffusion. Similar Cr distribution was observed in the LSCF/YSZ half cell using a bare E-brite alloy as interconnect [18]. Taniguchi et al. [34] also observed Cr_2O_3 deposition at the cathode/electrolyte interface when a LSM cathode was in contact with various Cr-containing alloys and compounds; the deposits resulted in significantly reduced cathode activity. For the single cell with the $Co_{0.40}Fe_{0.60}$-plated Crofer 22 APU interconnect, the Cr content in the cathode side gradually increased from the YSZ electrolyte to the LSM current collector layer. But the maximum Cr content in the cathode was still lower than the minimum Cr content detected in the cathode of the single cell with the bare interconnect. The cell performance stability was improved significantly with the plated $Co_{0.40}Fe_{0.60}$ layer on the interconnect, as the Cr evaporation/migration from Crofer 22 APU to the cathode was effectively blocked due to the presence of the converted $CoFe_2O_4$ spinel coating layer.

Table 3
EDS analysis of Cr content (wt.%) in the LSM cathode operated with the bare and $Co_{0.40}Fe_{0.60}$-plated Crofer 22 APU alloy interconnects, respectively. The analysis was conducted on the selected areas as indicated in Fig. 8.

Interconnect	Cr content (wt.%)			
	Region #1	Region #2	Region #3	Region #4
Bare alloy	0.19	1.62	1.42	0.51
Plated alloy	0.15	0.34	0.37	0.42

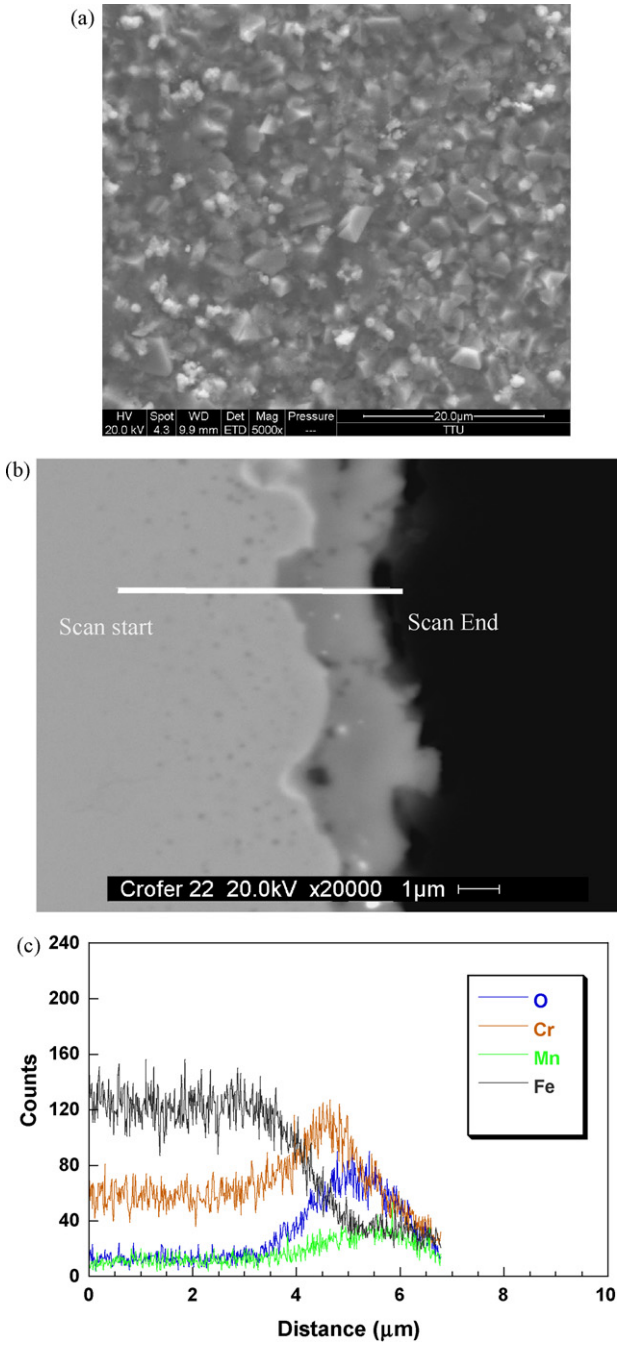

Fig. 9. Surface morphology (a), cross-sectional view (b), and EDS line scan (c) of the oxide scale formed on the bare interconnect after cell testing at 800 °C.

3.4. Surface morphology and structure of the thermally grown oxide scale

The surface morphology and cross-sectional analysis of the oxide scale formed on the bare and $Co_{0.40}Fe_{0.60}$-plated steel interconnects after cell testing are shown in Figs. 9 and 10, respectively. As shown in Fig. 9(a), some coarse octahedral spinel crystallites were embedded in the fine scale matrix for the bare Crofer 22 APU interconnect, similar to the results reported by Yang et al. [35]. Fig. 9(b) is the cross-sectional view of the oxide scale, while the corresponding EDS line scan is given in Fig. 9(c). It can be seen that a duplex oxide scale consisting of a Cr_2O_3 inner layer and a $(Mn,Cr,Fe)_3O_4$ outer layer was thermally grown on the bare substrate, as expected for Crofer 22 APU exposed to the cathode environment [35].

As shown in Fig. 10(a), the oxide scale on the $Co_{0.4}Fe_{0.6}$-plated steel surface was quite dense and compact. From Fig. 10(b) and (c), the oxide scale thermally grown on the plated interconnect comprised a 50-μm Cr-free $CoFe_2O_4$ spinel outer layer, a thin Cr_2O_3 inner layer, and a porous 8-μm Co-rich Mn–Fe–Cr–Co–O mixed oxide layer in between. The composition of the outer spinel layer was relatively uniform from the surface to the porous middle layer; no Cr and Mn could be detected in this layer, implying that the $Co_{0.40}Fe_{0.60}$ precursor alloy film could quickly and effectively be converted to $CoFe_2O_4$ in the SOFC cathode environment.

From the comparison of the cross-sections of the plated and bare interconnects, it is expected that the area-specific resistance of the unplated interconnect should be lower than that of the plated interconnect due to the thicker oxide scale and the presence of a porous middle layer for the plated interconnect. In the contrast, the power density of the single cell with the plated interconnect was much higher than that with the bare interconnect. Since a larger amount of Cr species deposit was found at the electrolyte/cathode

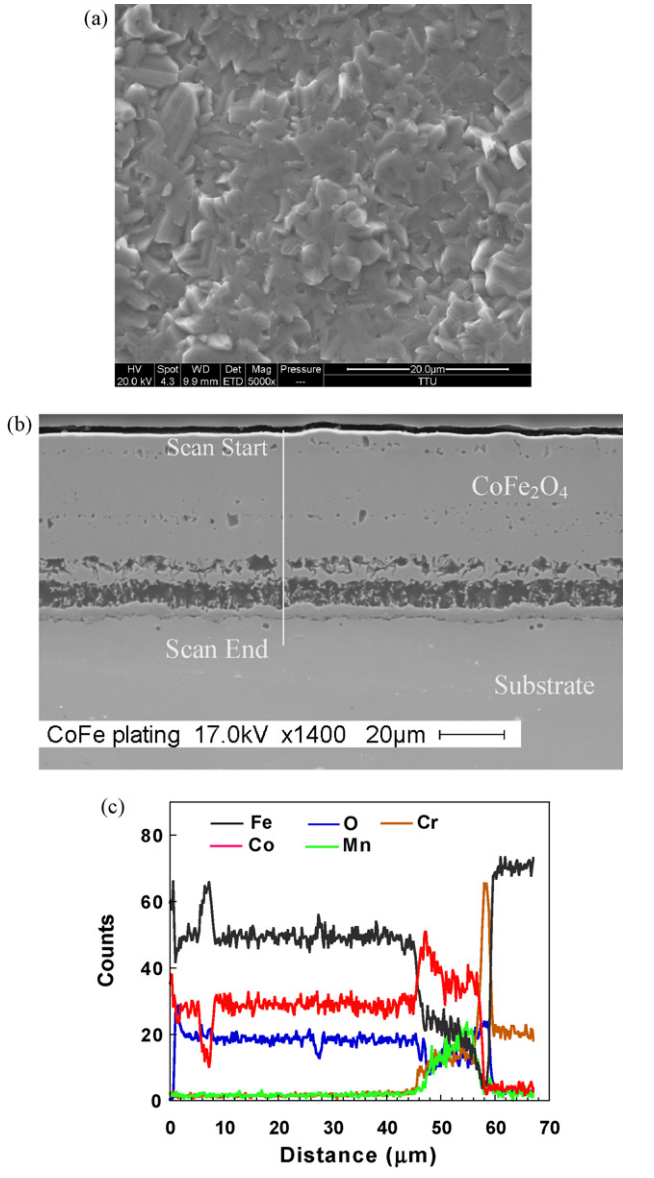

Fig. 10. Surface morphology (a), cross-sectional view (b), and EDS line scan (c) of the oxide scale formed on the plated interconnect after cell testing at 800 °C.

interface for the cell with the bare interconnect, the electrochemical active sites near the interface was more severely deactivated by the Cr species. Thus, Cr poisoning probably is a more important factor than the conductivity of the oxide scale in controlling the cell performance for these cells.

While a relatively thick oxide scale was formed on the plated interconnect, there was no signs of scale spallation after 300-h cell testing except near the edge of the interconnect channel, as a result of the excellent match in CTE of the $CoFe_2O_4$ spinel outer layer with the substrate alloy as well as the absence of severe thermal cycling. The adhesion of the coating might be further improved by the use of a thinner Co–Fe alloy layer, interdiffusion annealing of the plated interconnect after electrodeposition in a reduced environment, and/or controlled conversion treatment to form the spinel layer.

The combined results of cell testing and cross-sectional analysis suggest that Cr migration/transport could be effectively blocked by the formation of a dense, Cr-free $CoFe_2O_4$ spinel layer thermally converted from the electrodeposited $Co_{0.40}Fe_{0.60}$ alloy on the ferritic steel, thus improving the cell performance stability in the presence of a Cr-containing interconnect alloy.

4. Conclusions

The electrical conductivity and CTE of the $CoFe_2O_4$ spinel were measured in air at typical SOFC operating temperatures. These results suggest that $CoFe_2O_4$ is a potential protective coating spinel for the Cr_2O_3-forming stainless steel interconnects. The $CoFe_2O_4$ spinel coating could be attained by oxidizing the co-deposited $Co_{0.40}Fe_{0.60}$ alloy film at 800 °C in air. Furthermore, in cell testing the channeled Crofer 22 APU interconnect with the plated $Co_{0.40}Fe_{0.60}$ alloy film resulted in much higher cell performance and lower degradation rate than the bare interconnect due to the formation of a Cr-free $CoFe_2O_4$ spinel layer during cell testing. Electrodeposition of an alloy precursor layer followed by its thermal conversion to conductive spinel layer in the SOFC cathode environment provides an alternative way for fabricating electrically conductive, Cr-blocking spinel coating onto the Cr-containing ferritic steel interconnect.

Acknowledgements

This research was sponsored by NSF under DMR-0238113. Part of the work was also supported by the DOE UCR Program under Grant #DE-FG26-05NT42533.

References

[1] W.J. Quadakkers, J. Piron-Abellan, V. Shemet, L. Singheiser, Mater. High Temp. 20 (2003) 115–127.
[2] P. Singh, N.Q. Minh, Int. J. Appl. Ceram. Technol. 1 (2004) 5–15.
[3] S.J. Geng, J.H. Zhu, J. Power Sources 160 (2006) 1009–1016.
[4] K. Huang, P.Y. Hou, J.B. Goodenough, Solid State Ionics 129 (2000) 237–250.
[5] T. Harita, Y. Xiong, K. Yamaji, N. Sakai, H. Yokokawa, J. Power Sources 131 (2004) 293–298.
[6] Z. Yang, K.S. Weil, D.M. Paxton, J.W. Stevenson, J. Electrochem. Soc. 150 (2003) A1188–A1201.
[7] T. Kadowaki, T. Shiomitsu, E. Matsuda, H. Nakagawa, H. Tsuneizumi, Solid State Ionics 67 (1993) 65–69.
[8] J. Fergus, Mater. Sci. Eng. A 397 (2005) 271–277.
[9] W.Z. Zhu, S.C. Deevi, Mater. Res. Bull. 38 (2003) 957–972.
[10] W.J. Quadakkers, H. Greiner, M. Hansel, A. Pattanaik, A.S. Khanna, W. Mallener, Solid State Ionics 91 (1996) 55–67.
[11] K. Fujita, K. Ogasawara, Y. Matsuzaki, T. Sakurai, J. Power Sources 131 (2004) 261–269.
[12] Y. Larring, T. Norby, J. Electrochem. Soc. 147 (2000) 3251–3256.
[13] Z. Yang, G. Xia, J.W. Stevenson, Electrochem. Solid-State Lett. 8 (2005) A168–A170.
[14] X. Chen, P.Y. Hou, C.P. Jacobson, S.J. Visco, L.C. De Jonghe, Solid State Ionics 176 (2005) 425–433.
[15] Z.G. Yang, Int. Mater. Rev. 53 (2008) 39–54.
[16] X. Montero, F. Tietz, D. Sebold, H.P. Buchkremer, A. Ringuede, M. Gassir, A. Laresgoiti, I. Villarreal, J. Power Sources 184 (2008) 172–179.
[17] X.H. Deng, P. Wei, M.R. Bateni, A. Petric, J. Power Sources 160 (2006) 1225–1229.
[18] X.G. Li, J.W. Lee, B.N. Popov, J. Power Sources 187 (2009) 356–362.
[19] M.R. Bateni, P. Wei, X.H. Deng, A. Petric, Surf. Coat. Technol. 201 (2007) 4677–4684.
[20] P. Wei, X.H. Deng, M.R. Bateni, A. Petric, Corrosion 63 (2007) 529–535.
[21] P. Wei, X.H. Deng, M.R. Bateni, A. Petric, ECS Trans. 7 (2007) 2135–2143.
[22] J.W. Wu, Y.L. Jiang, C.D. Johnson, X.B. Liu, J. Power Sources 177 (2008) 376–385.
[23] J.W. Wu, C.D. Johnson, Y.L. Jiang, R.S. Gemmen, X.B. Liu, Electrochim. Acta 54 (2008) 793–800.
[24] J.W. Wu, C.D. Johnson, R.S. Gemmen, X.B. Liu, J. Power Sources 189 (2009) 1106–1113.
[25] D.Y. Park, B.Y. Yoo, S. Kelcher, N.V. Myung, Electrochim. Acta 51 (2006) 2523–2530.
[26] N. Mattoso, V. Fernandes, M. Abbate, W.H. Schreiner, D.H. Mosca, Electrochem. Solid-State Lett. 4 (2001) C20–C22.
[27] H. Ling, A. Petric, Proceedings of the 9th International Symposia on Solid Oxide Fuel Cells (SOFC-IX), vol. 2005–07, The Electrochemical Society, Pennington, NJ, USA, 2005, p. 1866.
[28] A. Petric, H. Ling, J. Am. Ceram. Soc. 90 (2007) 1515–1520.
[29] T. Kiefer, M. Zahid, F. Tietz, D. Stöver, H.-R. Zerfass, Proceedings of 26th Risø International Symposium on Materials Science: Solid State Electrochemistry, Roskilde, Denmark, 2005, p. 261.
[30] P.D. Jablonski, D.E. Alman, Int. J. Hydrogen Energy 32 (2007) 3705–3712.
[31] E.M. Kakuno, D.H. Mosca, I. Mazzaro, N. Mattoso, W.H. Schreiner, M.A.B. Gomes, J. Electrochem. Soc. 144 (1997) 3222–3226.
[32] S.P. Simner, M.D. Anderson, L.R. Pederson, J.W. Stevenson, J. Electrochem. Soc. 152 (2005) A1851–A1859.
[33] Y. Matsuzaki, I. Yasuda, Solid State Ionics 132 (2000) 271–278.
[34] Y.S. Taniguchi, M. Kadowaki, H. Kawamura, T. Yasuo, Y. Akiyama, Y. Miyake, J. Power Sources 55 (1995) 73–79.
[35] Z.G. Yang, M.S. Walker, P. Singh, J.W. Stevenson, T. Norby, J. Electrochem. Soc. 151 (2004) B669–B678.